Key Points:
- We invert the rupture process for both of the 2019 M_w 7.7 and 2000 M_w 8.0 earthquakes by using optical images and teleseismic waveforms
- The 2019 M_w 7.7 earthquake ruptured the northwestern continuation of the Weitin fault while the 2000 M_w 8.0 earthquake broke the southeast part
- The 2019 M_w 7.7 earthquake was more probably driven by the dynamic stresses during the southward propagation of the rupture front

Supporting Information:
- Supporting Information S1
- Data Set S1
- Data Set S2
- Data Set S3
- Data Set S4

Correspondence to:
K. Chen,
whuckj@gmail.com

The Weitin Fault, Papua New Guinea, Ruptured Twice by M_w 8.0 and M_w 7.7 Earthquakes in 2000 and 2019

Kejie Chen[1,2] , **Chris Milliner[3]** , and **Jean-Philippe Avouac[1]**

[1]Division of Geological and Planetary Sciences, California Institute of Technology, Pasadena, CA, USA, [2]Department of Earth and Space Sciences, Southern University of Science and Technology, Shenzhen, Guangdong, China, [3]Jet Propulsion Laboratory, California Institute of Technology, Pasadena, CA, USA

Abstract We determine the fault geometry and kinematic slip models of the 2019 M_w 7.7 and 2000 M_w 8.0 earthquakes in Papua New Guinea using measurements from optical image correlation and teleseismic waveforms. The 2000 earthquake ruptured an extensive fault system over a distance of ~150 km including the entire 60-km long onshore segment of the Weitin fault and its offshore continuation southeast of New Ireland. The northern portion of the onshore Weitin fault segment ruptured again in 2019. Most of the moment was released by a compact, shallow, high stress-drop slip patch on the northwestern continuation of the Weitin fault in the Saint George Channel, which was brought closer to failure by the 2000 earthquake. The two ruptures overlap over about 20 km but in fact mostly complement each other. Large dynamic stresses may have driven the partial rerupture of the Weitin fault during the 2019 event.

Plain Language Summary The Weitin Fault runs across the southern tip of New Ireland, Papua New Guinea and marks the boundary between the Bismark and the Pacific plate with an interseismic slip rate of ~13 cm/year. On May 14, 2019, it produced a M_w 7.7 earthquake, which according to our optical image correlation results, ruptured the surface for over 30 km and slipped by up to 5 m in a left-lateral sense. Optical image correlation measurements also show that a previous large earthquake, the M_w 8.0 event in 2000, had ruptured the entire 60-km onshore segment of the same fault. We use the optical image correlation results and seismological records to produce slip models of the two events to understand how the earlier event may have affected the most recent one. The 2019 earthquake was an unusually compact high stress-drop (~35 MPa) event, which ruptured an area that was brought closer to failure by the earlier 2000 earthquake but was energetic enough to propagate into the 2000 rupture area over 20 km.

1. Introduction

How successive ruptures along the same fault segment vary or not in the amount of slip and overall slip distribution can provide important insight into earthquake mechanics. Whether they arrest or initiate at geometric complexities, stay confined to the same area brought closer to failure by previous events, or overlap are features of particular interest (e.g., Harris et al., 1991; King et al., 1994; Wesnousky, 2006). However, due to the lack of direct and spatially complete observations of surface deformation, it is generally difficult to test whether earthquakes that occur adjacent to one another involve seismic ruptures with significant overlap or not. In addition, understanding whether the amount and overall distribution of slip is consistent from event-to-event or is more variable through time has significant implications for reconstructing slip distribution from past events that are only sparsely recorded in the geomorphology (Schwartz & Coppersmith, 1984; Zielke et al., 2015). Larger earthquakes ($M_w \geq 7$) are best suited for such analysis as their slip distributions might be constrained well enough from seismology, geodesy, and the observation of surface ruptures. Eastern Papua New Guinea (Figure 1) has been recognized to be a particularly suitable area for such studies due to the rapid relative plate motions and intense seismicity (Lay & Kanamori, 1980; Park & Mori, 2007a).

In a previous study, Park and Mori (2007a) studied five $M_w > 7.5$ blind thrust earthquakes that occurred between 1971 and 2000 along the plate boundary between the South Bismarck and the Solomon Sea plates. They found that the rupture areas overlapped but that the slip patterns were complementary to one another and concluded that asperities, defined as zone of high slip during seismic ruptures, are not persistent through time. Here we analyze two more recent earthquakes, of magnitude M_w 8.0 and M_w 7.7, which occurred close-by in 2000 and 2019, respectively, around the triple junction between the South Bismarck,
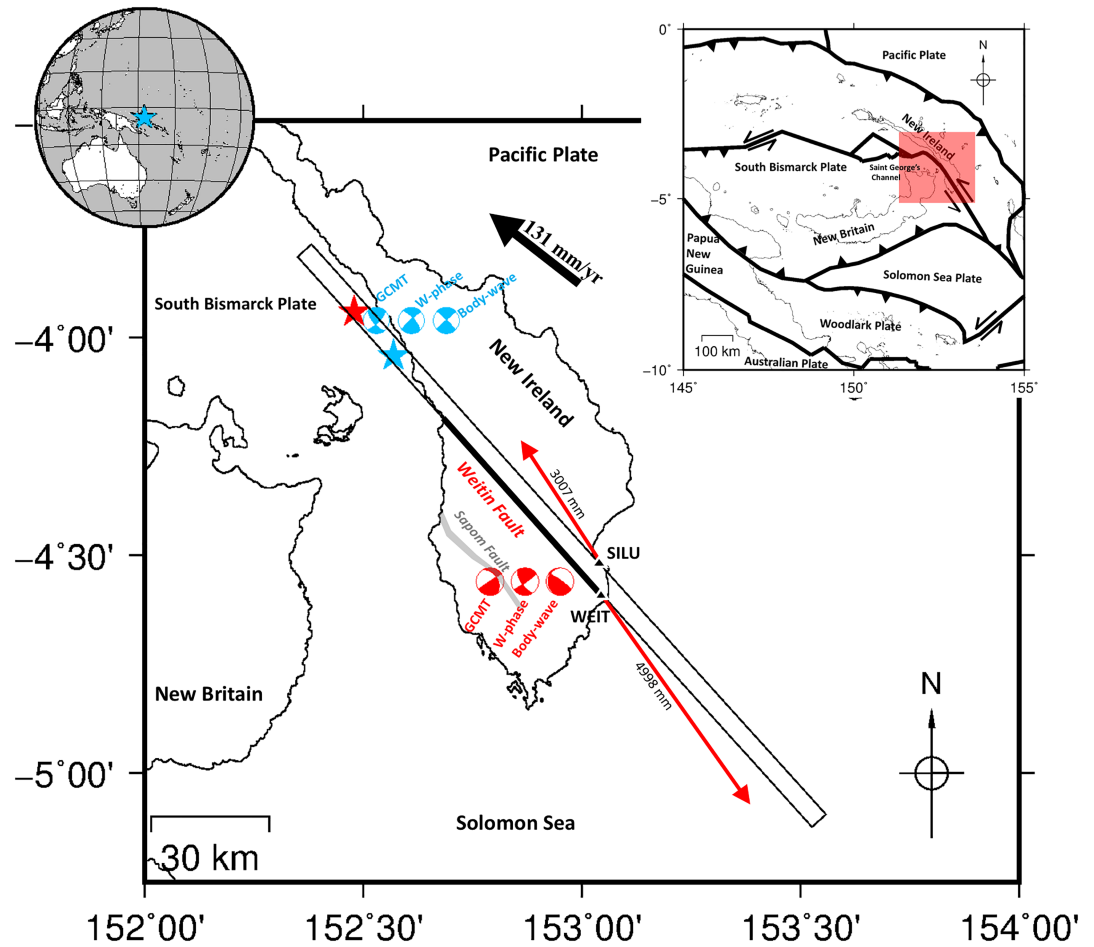
Figure 1. Simplified seismotectonic context of the 2000 M_w 8.0 and 2019 M_w 7.7 New Ireland earthquakes. Brief plate tectonic setting (top right inset map) is adopted from Tregoning et al. (1999), and the shaded red zone outlines the area of the main figure. Black thick line shows the approximate trace of the Weitin fault along the Weitin River (after Hohnen, 1978), and gray line indicates the Sapom fault trace. Red/blue stars/beachballs show epicenters and focal mechanisms of the 2000 M_w 8.0 and 2019 M_w 7.7 events, respectively. The epicenter of the 2000 M_w 8.0 event was inferred from Park and Mori (2007b), and the 2019 M_w 7.7 event epicenter was slightly adjusted from the USGS-NEIC solution. Focal mechanisms are Global CMT, USGS W-phase (Duputel et al., 2012) and body-wave solutions, and the GCMT focal mechanisms are placed at the centroid locations. Coseismic displacements (in red arrows) at two GPS stations SILU and NM40 caused by the 2000 M_w 8.0 earthquake are digitized from Tregoning et al. (2001). Black rectangle outlines the projection of the fault plane, which dips NE. Inset map (top right) shows the epicenter location from a global view.

Solomon Sea, and the Pacific plates (Tregoning et al., 1998; Figure 1). These two earthquakes produced surface ruptures onshore New Ireland, which we were able to document from correlation of satellite optical images using the COSI-Corr software package (Leprince, Ayoub, et al., 2007; Leprince, Barbot, et al., 2007). We combine these measurements with seismic waveform modeling (e.g., Hartzell & Heaton, 1983; Kikuchi & Kanamori, 1982) to determine kinematic models that describe the time-evolution of fault slip during the seismic ruptures. Hereafter, we present our measurement and modeling results for the 2019 and 2000 earthquakes. We then discuss implications for earthquake mechanics.

2. Analysis of the 2019 M_w 7.7 New Ireland Earthquake

The U.S. Geological Survey National Earthquake Information Center shows that epicenter of the May 14, 2019 M_w, 7.7 earthquake lies on the offshore continuation of the Weitin fault (https://earthquake.usgs.gov/earthquakes/eventpage/us70003kyy/executive). The W-phase focal mechanism (https://earthquake.usgs.gov/earthquakes/eventpage/us70003kyy/moment-tensor) shows a dominantly strike-slip source,
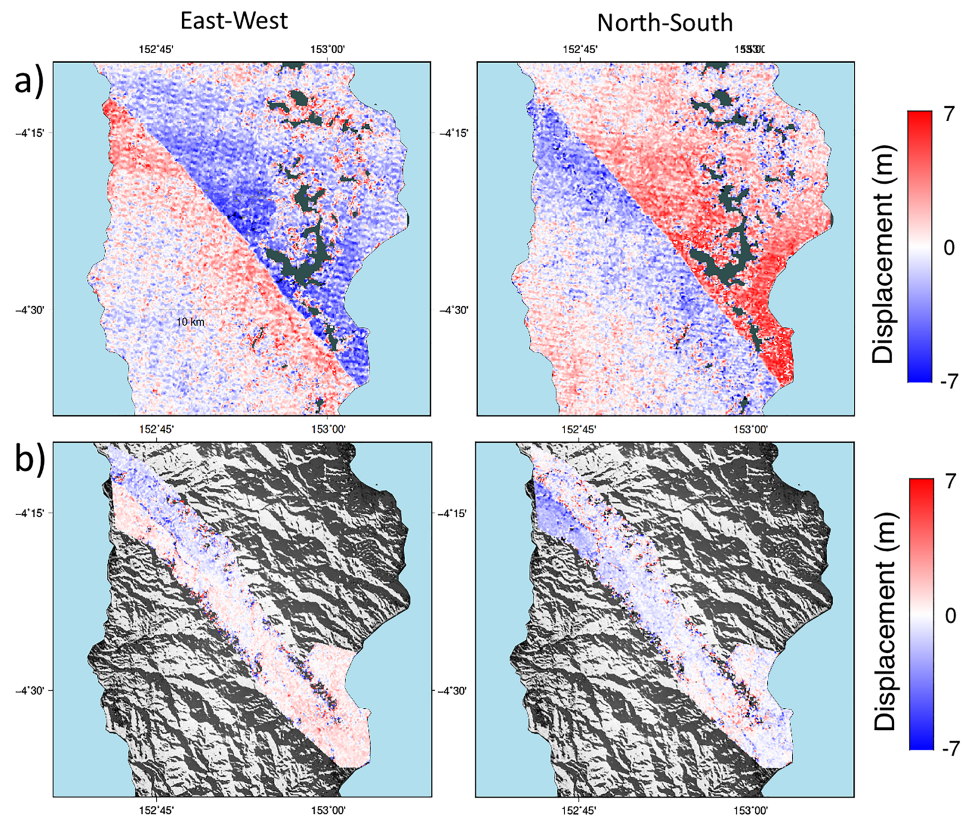
Figure 2. Surface ruptures due to the 2000 M_w 8.0 (a) and 2019 M_w 7.7 (b) earthquakes measured from coregistration and correlation of optical images using Landsat 7 and Sentinel 2 satellite images, respectively. See Table S1 for details of the images and acquisition dates.

consistent with left-lateral slip along the Weitin fault (Figure 1). We correlated Sentinel 2 optical images using a subpixel image correlator (see supporting information, Text S1 and supporting information, Table S1 for details of technique and imagery, Ayoub et al., 2009; Kääb et al., 2016; Leprince, Ayoub, et al., 2007; Leprince, Barbot, et al., 2007), which resolves the near-field horizontal surface displacement field. The correlation results (Figure 2a) show a clear discontinuity along 25 km of the northwest section of the Weitin fault with up to 4.2± 0.5 m of fault slip (Figure 3).

We also determined a finite source model of the rupture from the inversion of the teleseismic P and SH waveforms (see supporting information, Text S2 for information, Chen et al., 2019; Dziewonski & Anderson, 1981). We selected waveforms with a good azimuth coverage from Incorporated Research Institutions for Seismology and filtered them in the (0.005, 0.4) Hz frequency band. We assume a planar fault model with a strike and dip consistent with the surface ruptures along the Weitin fault and the W-Phase moment tensor. The fault strikes 318° and dips steeply (80°) to the northeast. We determined a best fitting source model using a least squares procedure with a specified rupture expansion speed using the multiple time window approach (Hartzell & Heaton, 1983). More detailed information is given in the supporting information. The solution obtained from inverting only the teleseismic P and SH waveforms yields a slip model roughly consistent with the measured slip at the surface (supporting information, Figure S3). The solution obtained by imposing the measured surface fault slip from optical image correlation on the shallowest subfault patches is thus very similar (supporting information, Figure S4). To assess the robustness and uncertainty of inversion results, we conducted a jackknife test by randomly removing 20% of data (see Text S2 and Figure S4). The jackknife test demonstrates that the overall slip pattern, concentrated predominantly within a 80-km long and 10-km deep fault portion, is well constrained, and the relative uncertainty on the cumulated slip estimate is about 10%. We conclude that the observed surface ruptures and the seismological data are consistent and that the surface slip measured from optical image correlation is probably mostly due to
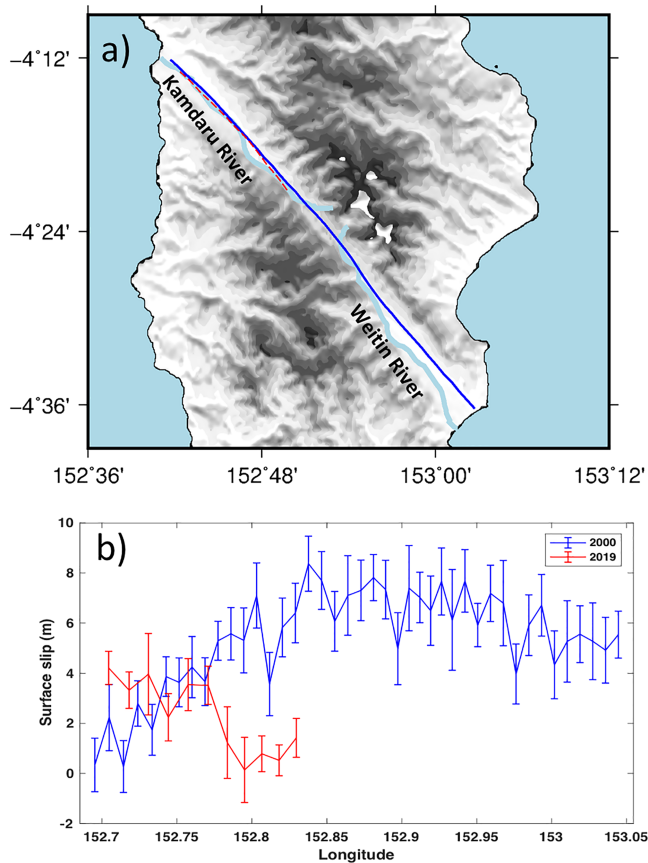
Figure 3. (a) Surface ruptures due to the 2000 M$_w$ 8.0 (blue) and 2019 M$_w$ 7.7 (red) earthquakes. (b) Comparison of surface fault slip for the 2019 M$_w$ 7.7 and 2000 M$_w$ 8.0 earthquakes.

seismic slip. We cannot exclude some contribution from shallow afterslip, which could be better resolved in future studies using postseismic geodetic time series analysis. The inferred source model reveals a very impulsive rupture, with a duration of only ~30 s for a total moment release of 4.8 × 10^{20} Nm (M$_w$ 7.7), and compact source, with a peak slip of ~25 m and a rupture area of about 50 × 10 km^2 (Figure 3). This source model implies a rather large stress drop of 35 MPa measured using the averaging procedure of Noda et al. (2013), and that the rupture propagated toward the surface along dip and bilaterally along strike, with a major portion of the energy released to the northwest.

Large strike-slip earthquakes on very linear fault segments may rupture at speeds faster than the shear wave velocity (e.g., Bao et al., 2018; Bouchon et al., 2001; Socquet et al, 2019). To test whether this earthquake was a supershear event, we run inversions with 2.8 and 3.8 km/s, but do not find significant changes either in the data fits or the slip distribution compared with a regular speed (2.8 km/s for the model shown in Figure 3). Our observations cannot confirm or exclude the possibility of a supershear rupture.

3. Analysis of the 2000, M$_w$ 8.0 New Ireland Earthquake

The M$_w$ 8.0 event in 2000 was in fact part of an earthquake sequence that lasted almost 2 months. It was already known from geodetic measurements that the Weitin faults had already ruptured during a sequence of large earthquakes in 2000 (Tregoning et al., 2005). This sequence lasted several months, which involved a M$_w$ 6.8 foreshock, the M$_w$ 8.0 New Ireland mainshock of November 16, 2000, and two M$_w$ ~7.5 aftershocks that activated the New Britain megathrust between the Solomon Sea and the Bismarck plates and the Weitin fault (Park & Mori, 2007b). Modeling of teleseismic waveforms of the M$_w$ 8.0 mainshock event suggests strike-slip and thrust motion on a fault striking 320° and dipping by 70° to the northeast roughly consistent with reactivation of the Weitin fault (Park & Mori, 2007b).

Measurements at two campaign GPS stations on each side of the fault and separated by <13 km show 8 m of left-lateral relative displacement (Tregoning et al., 2001; Tregoning et al., 2005; reported also in Figure 1). Vertical displacements are also consistent with a causative fault dipping to the northeast, where the site northeast of the Weitin fault was uplifted by ∼18 cm, while the site to the southwest subsided by ∼26 cm. Postseismic measurements revealed small postseismic displacement, but as the data were acquired starting only 2 days after the mainshock, the measured 8 m of slip is likely dominantly coseismic.

To constrain the surface deformation pattern and rupture extent of the 2000 earthquake, we used the same image correlation technique we applied to the most recent 2019 event (see Text S1 for processing details). Using Landsat 7 images acquired on 05/13/2000 and 05/06/2003, we find that the 2000 event ruptured the entire length of the Weitin fault that is exposed on New Ireland (for ~61 km), with up to 8.3± 1.2 m of left-lateral slip (Figures 2b and 3). These geodetic observations confirm left-lateral slip of the Weitin fault between May 2000 and May 2003. Furthermore, GPS repeat observations at station WEIT after the event (location shown in Figure 1) show only ~30 mm postseismic relaxation in 50 days (Tregoning et al., 2001). Considering the postseismic rate decreases exponentially, the contribution of overall postseismic slip is expected to be negligible compared to the ~5 m of coseismic slip. In the absence of any other large strike-slip event that could explain the surface ruptures (between the November 2000 earthquake and the postoptical image in May 2003), it is likely that displacements measured from the optical image correlation are mostly due to the M$_w$ 8.0 mainshock. We then use these optical data to constrain the source model of the 2000 event that inverted from teleseismic waveforms. The epicenter determined by the U.S. Geological Survey (https://earthquake.usgs.gov/earthquakes/eventpage/usp000a3qq/executive) lies in the Saint George Channel
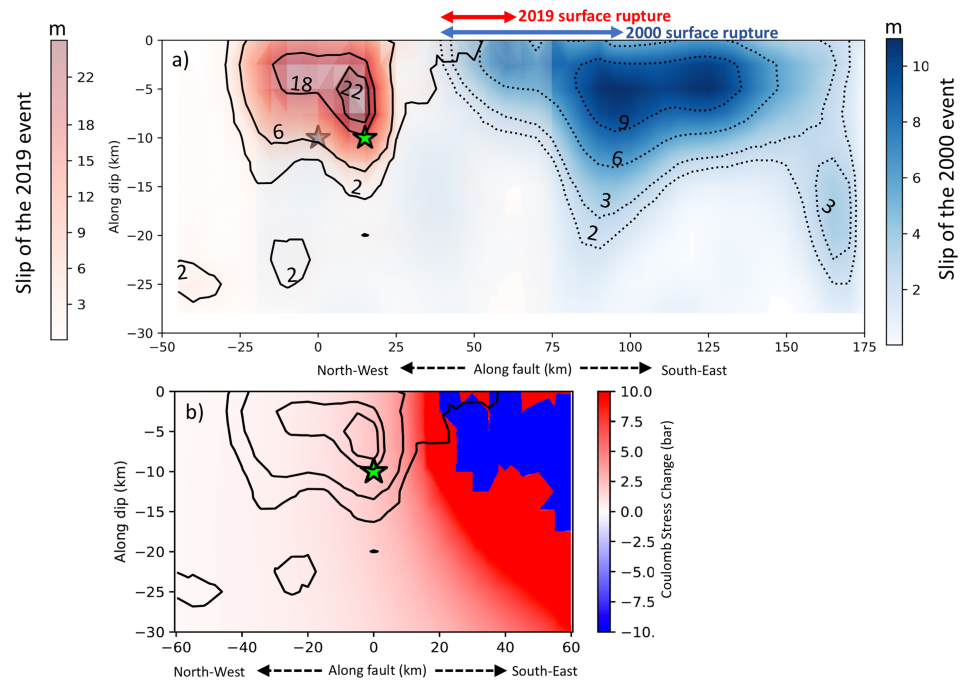
Figure 4. (a) Slip distribution of the 2019 M_w 7.7 (in red) and 2000 M_w 8.0 (in blue) earthquakes inverted from teleseismic P and SH waves and constrained with the optical image correlation results. The green and blue stars show their epicentres. Moment rate function and waveform fits are shown in supporting information, Figures S3 and S4. The Y-axis is rescaled by a factor of 3.5. (b) Coulomb stress change in the rupture area (outlined by the black contour lines) of the 2019 M_w 7.7 earthquake induced by the 2000 M_w 8.0 earthquake, the green star marks the epicentre of the 2019 event. The colorbar is saturated. The slip model was thresholded at 1.5 m to avoid spurious values in areas with poorly resolved slip.

between New Britain and New Ireland, which relative to the expected source size, is located surprisingly far from the W-Phase centroids (Figure 1). It is therefore likely that the earthquake initiated on a separate fault that then triggered rupture of the Weitin fault later on. This would also explain the rather emergent source-time function (Figure S4). Similar to Park and Mori (2007b), to model the main rupture of the Weitin fault, we consider a starting point on the northeastern continuation of the Weitin fault in the Saint George Channel, an assumption that is used to simplify the inversion procedure as only one fault can be considered. Furthermore, to keep the fault geometry consistent with the 2019 M_w 7.7 event, the strike/dip angles are set to at 318°/80°, which are similar to the values proposed by Park and Mori (2007b), of 320°/70°.

Our source model for the 2000 event explains well the teleseismic and geodetic measurements (supporting information, Figure S5). We find a total moment release of ~1.09×10^{21} Nm (M_w 7.96), close to the W-phase solution but smaller than the value of M_w 8.2 obtained by Park and Mori (2007b) that was likely overestimated. The source model also indicates a long duration of the source time function (60 s) with a rupture velocity of 2.8 km/s. Both our inversion and Park and Mori's (2007b) model show little moment released near the hypocenter and a significant thrust component on the major slip patch. Unlike the 2019 M_w 7.7 event, this earthquake propagated almost unilaterally to the southeast. Besides, using the same fault geometry and same level of smoothing, the peak slip (~10 m) is only half of the 2019 M_w 7.7 earthquake, indicating the 2019 event is much more impulsive and compact.

We notice that for the 2000 and 2019 events, rather diverse focal mechanisms have been reported (see Figure 1). To assess the impact of the choice of the dip angle on the slip models, we run a series of inversions using dipping angles from 45° to 85° with a step of 5° (see supporting information, Figure S2). We also run inversions with reported focal mechanisms. For the 79° NE dip angle, we find that the solution has nearly a pure thrust component and for the 43° NE dip angle, nearly pure strike-slip. Both of these solutions yield a poor fit to the data and thus can be excluded. In spite of the GPS coseismic offsets (see Figure 1), which favor

a NE dipping fault plane for the 2000 event, we also tested a SW dipping fault at 68° and found that the basic rupture features (including slip amount and distribution) remain persistent (see supporting information, Figure S6 where the fit of the seismic waveforms is slightly worse than the for the steep NE dipping fault planes). Although the diverse focal mechanisms and the noncouple components of some moment tensor solutions indicate the earthquake source may more complicated than that represented by a simple planar fault, the inversion tests show that the overall amount and distribution of fault slip, especially at shallow depths (<10 km), that is largely constrained by the optical measurements, is insensitive and is a robust feature.

4. Discussion and Conclusion

Our study demonstrates that the Weitin fault ruptured both in 2000 and 2019, producing each time 3–4 m of slip along the 20-km long portion where the ruptures overlap (Figures 3 and 4a). Such overlaps are rare, but this example is not unique. There are indeed previous instances of successive earthquakes separated by a short time interval producing overlapping ruptures. For example, the surface ruptures from the M_w 7.4 Izmit and the M_w 7.1 Duzce earthquakes, which occurred on the North Anatolia fault only 3 months apart in 1999, overlap over 10 km with 1–2 m of slip in each event (Konca et al., 2010). The rupture front of the Izmit earthquake, the first event in the sequence, arrested in the zone of overlap. Another notable example is the M_w 6.6 1979 earthquake in the Imperial Valley, which ruptured a ~30-km long fault segment that had already ruptured during the M_w 7.0 El Centro earthquake of 1940 as part of larger, ~60-km long rupture (Rockwell & Klinger, 2013). Slip was of the order of 50 cm to 1 m in each event. Recently, using back projection, Vallée and Satriano (2014) demonstrated that the 2013 M_w 7.8 Scotia Sea earthquake propagated into a 100-km long zone, which had already ruptured in a M_w 7.6 earthquake in 2003. Other examples of overlapping ruptures include the 1981 Sirch and 1998 Fandoqa earthquakes in Iran (Berberian et al., 2001), the 2016 M_w 7.3 Kumamoto, Japan earthquake, which ruptured a fault that had already ruptured during a M_w 6.5 foreshocks 2 days earlier (Sugito et al., 2016), and the 2017 Hojedk triplet, Iran, which ruptured a shallow dipping thrust fault that then reruptured two more times, 12 days apart, during the second and third earthquakes (Savidge et al., 2019). The slip models obtained from the inversion of the teleseismic waveforms using the constraints from remote sensing show the 2019 and 2000 slip distribution actually mostly complement each other (Figure 4a), as is also the case with the Izmit and Duzce ruptures (Konca et al., 2010). In both cases, the overlap was relatively small compared to the rupture lengths of these events (<10%). This suggests that even though there may be little elastic accumulation between events, it is possible that the same fault segment may rerupture with significant slip and that segments of faults do not exclusively fail by similar types of event.

In order to shed some light on the relationship between the two Papua New Guinea events and the reason for the overlap, we have calculated the Coulomb Failure stress changes (King et al., 1994) induced by the 2000 rupture on the Weitin fault (Figure 4b). Without setting a threshold in the slip model below which we ignore slip to calculate Coulomb Failure stress, the pattern of Coulomb stress changes is quite messy. We found that a threshold of 1.5 m does not impact the fit to the seismological waveforms (see supporting information, Figure S7) and produces a much cleaner distribution of Coulomb stress changes. The static stress calculation shows that most of the 2019 rupture occurred in an area where the Coulomb stress increased by a few bars due to the 2000 event. Furthermore, the static stress model also shows that the 2019 rupture was able to propagate into a region where the stress drop exceeded 1 MPa in the 2000 event. Since 2000, the interseismic loading has likely further loaded this stress drop region, but in the absence of good geodetic constraints, an interseismic strain rate cannot be estimated accurately. However, assuming the interseismic loading rate is typically of the order of kPa/year, such an amount is unlikely to have completely compensated the large stress drop that occurred in the 2000 event.

Assuming that the fault has remained locked since 2000, the proposed 13 cm/year slip rate (Tregoning et al., 1998) on the fault implies at most 2.5 m of slip deficit, which is less than the slip observed in 2019 on the northern segment of the Weitin fault. The stress drop there could have been incomplete in 2000, leaving some stresses to be released in 2019. This would contrast with the analysis of Tregoning et al. (2005) who noticed very little aftershock activity along the Weitin fault following the 2000 event. They interpreted this feature as an indication of complete stress release during the 2000 New Ireland earthquake sequence. We

infer that the 2019 rupture was more likely driven by the dynamic stresses during the southward propagation of the rupture front. The very compact and high stress-drop source characteristics of the 2019 event suggested by the body waves analysis indicate that the dynamic stresses may have been particularly high. Note that this explanation would not explain the Imperial Valley doublet: The 1979 rupture was entirely confined within the 1940 rupture and could not have been driven by dynamic stresses coming from a rupture beyond the limits of the 1940 events.

The rupture in 2019 arrested along a linear and structurally simple portion of the Weiten fault (Figure 3). Close inspection of the morphology in the area of the southern termination of the 2019 rupture shows there could be a slight subsegment boundary in this region. The area corresponds with a topographic saddle, where the valley becomes narrower, quaternary sediments pinch out (Hohnen, 1978), and marks a boundary in the watershed where it separates the Kamdaru river that flows northwest and the Weitin river that flows southeast (Figure 3). However, there is still no clear expression of any fault structural complexity. We note that the optical image measurements show very linear fault geometry both in the 2019 and 2000 ruptures. Therefore, the fault geometry, which for most ruptures is found to coincide with the terminations (e.g., Wesnousky, 2006), is unlikely to have been a contributing factor to impeding the 2019 rupture. The low prestress on the Weitin fault due to the previous 2000 event is probably the main factor that contributed in arresting the southward propagation during the 2019 event.

The cause of the northwestern termination of the 2000 event, located offshore in the Saint George Channel, which subsequently slipped by up to 24 m in 2019, is unclear. One possible explanation is that the stress level must have been high on that fault segment already in 2000. The <2.5-m slip deficit accrued since 2000 accounts for only a small fraction (<20%) of the slip observed in 2019. It is therefore surprising that this fault segment did not fail in the 2000 event. Future studies based on dynamic modeling of these two events could help elucidate the mechanisms that could explain why the 2000 rupture did not propagate fully into the Saint George Channel. Dynamic modeling would also bring insight on the frictional properties needed to explain the 20-km overlap between the two ruptures. We propose that intense dynamic weakening, as can result, for example, from pore pressurization or thermal pressurization (e.g., Noda & Lapusta, 2013), could explain the high stress-drop in 2019 offshore where the 2000 rupture terminated, as well as the propagation of the rupture into the segment of overlap that had already ruptured in 2000 where prestresses were presumably low.

References

Ayoub, F., Leprince, S., & Avouac, J. P. (2009). Co-registration and correlation of aerial photographs for ground deformation measurements. *ISPRS Journal of Photogrammetry and Remote Sensing*, *64*(6), 551–560. https://doi.org/10.1016/j.isprsjprs.2009.03.005

Bao, H., Ampuero, J., Meng, L., Fielding, E. J., Liang, C., Feng, T., & Huang, H. (2018). Early and persistent supershear rupture of the 2018 Mw 7.5 Palu earthquake Han. *Nature Geoscience*, 1–21. https://doi.org/10.31223/OSF.IO/TUASF

Berberian, M., Jackson, J. A., Fielding, E., Parsons, B. E., Priestley, K., Qorashi, M., et al. (2001). The 1998 March 14 Fandoqa earthquake (Mw 6.6.) in Kerman province, Southeast Iran: Re-rupture of the 1981 Sirch earthquake fault, triggering of slip on adjacent thrusts and the active tectonics of the Gowk fault zone. *Geophysical Journal International*, *146*(2), 371–398. https://doi.org/10.1046/j.1365-246X.2001.01459.x

Bouchon, M., Bouin, M. P., Karabulut, H., Nafi Toksöz, M., Dietrich, M., & Rosakis, A. J. (2001). How fast is rupture during an earthquake? New insights from the 1999 Turkey earthquakes. *Geophysical Research Letters*, *28*(14), 2723–2726. https://doi.org/10.1029/2001GL013112

Chen, K., Liu, Z., & Song, Y. T. (2019). Automated GNSS and teleseismic earthquake inversion (AutoQuake Inversion) for tsunami early warning: retrospective and real-time results. *Pure and Applied Geophysics*, 1–21. https://doi.org/10.1007/s00024-019-02252-x

Duputel, Z., Rivera, L., Kanamori, H., & Hayes, G. (2012). W phase source inversion for moderate to large earthquakes (1990-2010). *Geophysical Journal International*, *189*(2), 1125–1147. https://doi.org/10.1111/j.1365-246X.2012.05419.x

Dziewonski, A. M., & Anderson, D. L. (1981). Preliminary reference Earth model. *Physics of the Earth and Planetary Interiors*, *25*(4), 297–356. https://doi.org/10.1016/0031-9201(81)90046-7

Harris, R., Archuleta, R., & Day, S. (1991). Fault steps and the dynamic rupture process: 2-D numerical simulations of a spontaneously propagating shear fracture. *Geophysical Research Letters*, *18*(5), 893–896. https://doi.org/10.1029/91GL01061

Hartzell, S. H., & Heaton, T. H. (1983). Inversion of strong ground motion and teleseismic waveform data for the fault rupture history of the 1979 Imperial Valley, California, earthquake. *Bulletin of the Seismological Society of America*, *73*(6), 1553–1583. https://doi.org/10.1016/0040-1951(87)90022-9

Hohnen, P. D. (1978). Geology of New Ireland, Papua New Guinea, *Australia Bureau of Mineral Resources Geology & Geophysics Bulletin*, *194*, 12.

Kääb, A., Winsvold, S. H., Altena, B., Nuth, C., Nagler, T., & Wuite, J. (2016). Glacier remote sensing using sentinel-2. part I: Radiometric and geometric performance, and application to ice velocity. *Remote Sensing*, *8*(7), 598. https://doi.org/10.3390/rs8070598

Kikuchi, M., & Kanamori, H. (1982). Inversion of complex body waves. *Bulletin of the Seismological Society of America*, *72*(2), 491–506.

King, G. C. P., Stein, R. S., & Lin, J. (1994). Static stress changes and the triggering of earthquakes. *Bulletin of the Seismological Society of America*, *84*(3), 935–953.

Konca, O. A., Leprince, S., Avouac, J. P., & Helmberger, D. V. (2010). Rupture process of the 1999 Mw 7.1 duzce earthquake from joint analysis of SPOT, GPS, InSAR, strong-motion, and teleseismic data: A supershear rupture with variable rupture velocity. *Bulletin of the Seismological Society of America*, *100*(1), 267–288. https://doi.org/10.1785/0120090072

Lay, T., & Kanamori, H. (1980). Earthquake doublets in the Solomon Islands. *Physics of the Earth and Planetary Interiors*, *21*(4), 283–304. https://doi.org/10.1016/0031-9201(80)90134-X

Leprince, S., Ayoub, F., Klinger, Y., & Avouac, J. P. (2007). Co-registration of optically sensed images and correlation (COSI-Corr): An operational methodology for ground deformation measurements, in *International Geoscience and Remote Sensing Symposium (IGARSS)*, https://doi.org/10.1109/IGARSS.2007.4423207

Leprince, S., Barbot, S., Ayoub, F., & Avouac, J. P. (2007). Automatic and precise orthorectification, coregistration, and subpixel correlation of satellite images, application to ground deformation measurements. *IEEE Transactions on Geoscience and Remote Sensing*, *45*(6), 1529–1558. https://doi.org/10.1109/TGRS.2006.888937

Noda, H., & Lapusta, N. (2013). Stable creeping fault segments can become destructive as a result of dynamic weakening. *Nature*, *493*(7433), 518–521. https://doi.org/10.1038/nature11703

Noda, H., Lapusta, N., & Kanamori, H. (2013). Comparison of average stress drop measures for ruptures with heterogeneous stress change and implications for earthquake physics. *Geophysical Journal International*, *193*(3), 1691–1712. https://doi.org/10.1093/gji/ggt074

Park, S. C., & Mori, J. (2007a). Are asperity patterns persistent? Implication from large earthquakes in Papua New Guinea. *Journal of Geophysical Research*, *112*, B03303. https://doi.org/10.1029/2006JB004481

Park, S. C., & Mori, J. (2007b). Triggering of earthquakes during the 2000 Papua New Guinea earthquake sequence. *Journal of Geophysical Research*, *112*, B03302. https://doi.org/10.1029/2006JB004480

Rockwell, T. K., & Klinger, Y. (2013). Surface rupture and slip distribution of the 1940 Imperial Valley earthquake, Imperial Fault, Southern California: Implications for rupture segmentation and dynamics. *Bulletin of the Seismological Society of America*, *103*(2A), 629–640. https://doi.org/10.1785/0120120192

Savidge, E., Nissen, E., Nemati, M., Karasözen, E., Hollingsworth, J., Talebian, M., et al. (2019). The December 2017 Hojedk (Iran) earthquake triplet—Sequential rupture of shallow reverse faults in a strike-slip restraining bend. *Geophysical Journal International*, *217*(2), 909–925. https://doi.org/10.1093/gji/ggz053

Schwartz, D. P., & Coppersmith, K. J. (1984). Fault behavior and characteristic earthquakes: Examples from the Wasatch and San Andreas fault zones (USA). *Journal of Geophysical Research*, *89*(B7), 5681–5698. https://doi.org/10.1029/JB089iB07p05681

Socquet, A., Hollingsworth, J., Pathier, E., & Bouchon, M. (2019). Evidence of supershear during the 2018 magnitude 7.5 Palu earthquake from space geodesy. *Nature Geoscience*, *12*(3), 192–199. https://doi.org/10.1038/s41561-018-0296-0

Sugito, N., Goto, H., Kumahara, Y., Tsutsumi, H., Nakata, T., Kagohara, K., et al. (2016). Surface fault ruptures associated with the 14 April foreshock (Mj 6.5) of the 2016 Kumamoto earthquake sequence, southwest Japan. *Earth Planets Space*, *68*(1), 1–8. https://doi.org/10.1186/s40623-016-0547-5

Tregoning, P., Jackson, R. J., McQueen, H., Lambeck, K., Stevens, C., Little, R. P., et al. (1999). Motion of the South Bismarck Plate, Papua New Guinea. *Geophysical Research Letters*, *26*(23), 3517–3520. https://doi.org/10.1029/1999GL010840

Tregoning, P., Lambeck, K., Stolz, A., Morgan, P., McClusky, S. C., van der Beek, P., et al. (1998). Estimation of current plate motions in Papua New Guinea from Global Positioning System observations. *Journal of Geophysical Research*, *103*(B6), 12,181–12,203. https://doi.org/10.1029/97JB03676

Tregoning, P., McQueen, H., Lambeck, K., Stanaway, R., Saunders, S., Itikarai, I., et al. (2001). Progress report on geodetic monitoring of the november 16, 2000 —New Ireland earthquake. Australian National University, Research School of Earth Sciences, Special Report 2001/3. http://rses.anu.edu.au/geodynamics/tregoning/RSES_SR_2001-3.pdf

Tregoning, P., Sambridge, M., McQueen, H., Toulmin, S., & Nicholson, T. (2005). Tectonic interpretation of aftershock relocations in eastern Papua New Guinea using teleseismic data and the arrival pattern method. *Geophysical Journal International*, *160*(3), 1103–1111. https://doi.org/10.1111/j.1365-246X.2005.02567.x

Vallée, M., & Satriano, C. (2014). Ten year recurrence time between two major earthquakes affecting the same fault segment. *Geophysical Research Letters*, *41*, 2312–2318. https://doi.org/10.1002/2014GL059465

Wesnousky, S. G. (2006). Predicting the endpoints of earthquake ruptures. *Nature*, *444*(7117), 358–360. https://doi.org/10.1038/nature05275

Wessel, P., Smith, W. H. F., Scharroo, R., Luis, J., & Wobbe, F. (2013). Generic mapping tools: Improved version released. *Eos Transactions American Geophysical Union*, *94*(45), 409–410. https://doi.org/10.1002/2013EO450001

Zielke, O., Klinger, Y., & Arrowsmith, J. R. (2015). Fault slip and earthquake recurrence along strike-slip faults—Contributions of high-resolution geomorphic data. *Tectonophysics*, *638*, 43–62. https://doi.org/10.1016/j.tecto.2014.11.004